Journal Name

Communication

Growth and dissolution of NaO_2 in an ether-based electrolyte, as the discharge product in the Na-O_2 cell

Iain M. Aldous and Laurence J. Hardwick

Received 00th January 20xx,
Accepted 00th January 20xx

DOI: 10.1039/x0xx00000x

www.rsc.org/

Deposition and dissolution of sodium superoxide (NaO_2) was investigated by atomic force microscopy. Rectangular prisms consisting of 8 smaller sub-structures grew from NaO_2 platelets, when discharged in 0.5 M $NaClO_4$, diethylene glycol dimethyl ether on highly ordered pyrolytic graphite. During oxidation the 8 sub-structures is conserved. 200 nm diameter ring-like structures of Na_2CO_3 remain at the end of oxidation.

The sodium-oxygen battery (Na-O_2) is under investigation due its advantageous theoretical specific energy of 1106 Wh kg^{-1} for the reaction (equation 1).[1]

$Na^+ + e^- + O_2 \rightarrow NaO_2$ $E^o = 2.27$ V vs. Na^+/Na (1)

The reduction of dissolved O_2 in the present of Na^+ results in the precipitation of large micrometre sized cubes (1 – 50 µm[2,3]) of NaO_2 on the surface of the electrode. Understanding the growth and dissolution mechanism of NaO_2 cubes formed from the one electron reduction of O_2 is critical towards the realisation of Na-O_2 as a practical technology. NaO_2 cubes are often of uniform size; however their morphology changes based on the rate of formation. At high rates (>600 µA cm^{-2})[2] icosahedral features are formed on the electrode surface.[2] At lower rates (<400 µA cm^{-2})[2] they precipitate out as cubes.[4] The explanation of these observations is that at higher rates the amount of soluble NaO_2 formed rapidly saturates the electrolyte near the electrode interface and precipitates out as smaller cubes at many nucleation points.[2] Whereas the slower formation and saturation of the electrolyte at lower rates forms larger cubes at a decreased amount of nucleation points. Subsequently the reaction is halted by the formation of compact, insulating NaO_2 films.[5,6]

Recent reports on the growth mechanism of NaO_2 suggest that the soluble formation of NaO_2, aided by HO_2[7] catalysed intermediates, agglomerate within the solution to form cubic structures.[7] The sudden death of the cell chemistry is attributed to the formation of a passivation film between the cube structures at the end of discharge process, which the thickness is discharge rate dependent.[8]

Although many factors upon NaO_2 growth and morphology have been reported including: rate[2,8,9], impurity concentration[7,10], and solvent dependence[11–18], a unified model of the fundamental control parameters of the discharge process remains unclear, with different conclusions operating under similar conditions being made. However, there has been an extensive review carried out by Bender *et al*[1] that ascertains the differences and similarities, Bi *et al*[19] analysed the cell setup concluding that glass cell setups obtain different discharge products (mainly $Na_2O_2.2H_2O$) to stainless steel cell setups (NaO_2 only).

Atomic force microscopy (AFM) is a powerful method for the investigation of NaO_2 growth and dissolution reaction, as size and morphology of the deposits can be directly measured with nm precision. This experimental approach has been already successfully undertaken in the lithium-oxygen (Li-O_2) battery system by Wen *et al*[20] on highly ordered pyrolytic graphite (HOPG) and Liu *et al*[21] on Au. On HOPG agglomerates of LiO_2 nanoparticles collect and grow at step edges forming Li_2O_2 nanoplates.[20] Upon Au, due to the lack of step edges and more uniform surface reactivity, Liu *et al*[21] concluded that a soluble LiO_2 species initially form that subsequently precipitates out on the surface as Li_2O_2.[22] S. E. Herrera *et al*[23] studied the formation of Li_2O_2 in DMSO on HOPG using *ex situ* AFM and herein an analogous AFM study in the Na-O_2 system of the growth and dissolution of NaO_2 precipitates upon HOPG is presented.

The CV of O_2 saturated 0.5 M $NaClO_4$, diethylene glycol dimethyl ether (DEGDME) on a HOPG surface is shown in Figure 1a. All stated potentials are vs. Na^+/Na. The reductive current rise begins at the thermodynamic potential of NaO_2 formation (2.33 V) where it peaks at 1.5 V.

During the reverse scan a broad peak beginning at 2.35 V,

Stephenson Institute for Renewable Energy, Department of Chemistry, University of Liverpool, Liverpool, L69 7ZD, UK

†Electronic Supplementary Information (ESI) available: Experimental Details, Line profiles from AFM images and Raman of NaO_2 deposits and FTIR characterisation of residual film after oxidation.. See DOI: 10.1039/x0xx00000x

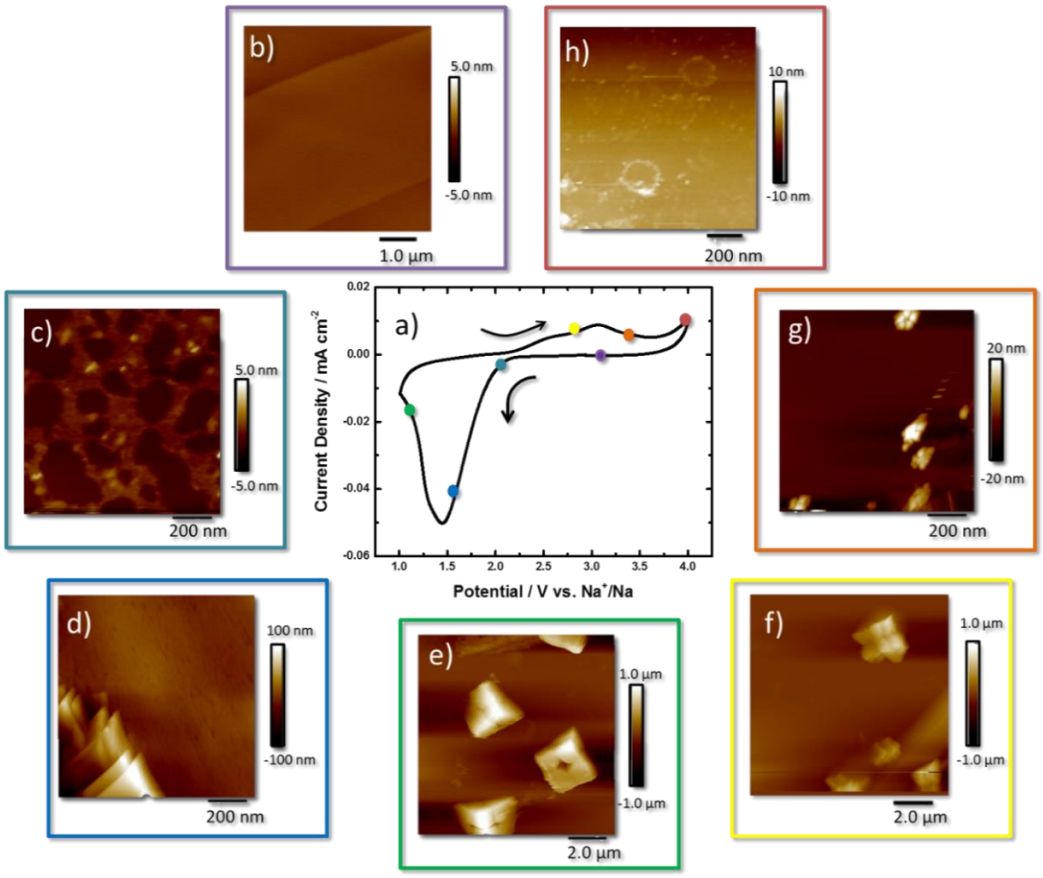

Figure 1. a) Cyclic voltammetry of HOPG in oxygen saturated, 0.5 M $NaClO_4$ DEGDME, AFM images taken at various potential around the CV b) 2.8, c) 2.10, d) 1.6, e) 1.1, f) 2.8, g) 3.3, h) 4.0 V vs. Na^+/Na.

reaching a maximum at 3.06 V, signals the electrooxidation of NaO_2 back to O_2 and Na^+. The current increases at 4.0 V suggesting further oxidation of remaining reaction products.[16,24,12]

The sequential description of the AFM images collected around the CV curve begins at OCP (2.8 V) where the small striations of the freshly cleaved HOPG surface are observed that follow the step edges of the stacked graphene sheets, the height profiles showing that the step edges are 0.8 nm in height (Figure 1b/Figure S1). At 2.2 V (Figure 1c) an inhomogeneous 5 nm film of NaO_2 was observed on the surface with 20x20 nm sized 5 nm thick deposits. Calculating the weight of the discharge product, via the charge passed, estimates an idealised film of 4.7 nm formed on the surface (Table S1). Height profiles are shown in the ESI for all measurements (Figures S2–S7).

The formation of 50-150 nm thick plate-like structures of NaO_2 were observed at 1.9 V (Figure 1d / Figure S3), and at 1.5 V the formation of cube-like NaO_2 crystals at the interface is observed (Figure 1e / Figure S4). The NaO_2 crystals have the dimensions of 2x2x1 µm, with axial lines visible on the surface along with a centralised recess that is half the deposits height. These deposits are smaller than those observed in the literature which are generally 2-10 µm in size.[25] Raman spectra (Figure S8) of these deposits show a peak at 1165cm^{-1}, consistent with a superoxide species. The axial lines reveal a structure whereby the discrete crystal consists of stacked particles that have agglomerated on the surface and grown together. Some crystals appear prismatic or tetragonal in shape coming out of the surface, but still contain the same axial lines defining different cube-like features together, but emerging out of plane. The depth of the hole within the centre of the crystal is ~0.5 µm in height as shown from the line profile (Figure S4).

Taking an extended view of the surface the NaO_2 crystals formed at the HOPG surface are all fairly uniform in size and are scattered both across the basal plane and agglomerated along the step edge (Figure S9).) Visible along x and y axis of these features are faint lines that reveal cubic building blocks of the overall structure (Figure 1e). The scale of the hole here suggests that the depth of this hole is in fact the height of the cube (1.0 µm). Upon closer inspection of the height profile it is actually 0.5 µm (Figure S4). For other deposits the electrode surface is visible in the middle of the cube (Figure S10). The secondary image taken on top of NaO_2 shows the imperfect facets of the cube structure. This is interesting as the majority of studies show uniform NaO_2 cubes that appear perfect plate like structures.[26]

Reversing the potential back to 2.6 V the NaO_2 are diminished in size with the axial outlines of smaller cubes making up the larger crystals still apparent (Figure 1f/Figure S7). This observation concurs with the previous state that these NaO_2 crystals formed are built essentially from 8 smaller

building blocks. By moving the over potential to 3.25 V (Figure 1g/Figure S8), beyond the peak current density of the redox process, very little NaO_2 is left upon the surface of the HOPG. Only tiny agglomerates of nanoparticles (ca. 20 nm in height) are observed. At 4.0 V little remains on the surface of the HOPG electrode (Figure 1h/Figure S9). Nonetheless, in comparison with HOPG at OCP (Figure 1b) the image shows some residual material on the electrode surface, some of which forms rings of ca. 200 nm diameter, 1.5-7 nm height, suggests incomplete oxidation of the discharge products. This is possibly imprints of NaO_2 deposits on the surface of the electrode (Line profile shown in Figure S9). The plates could be a coating of side products from other reactions as indicated by Ledano *et al*[26] and Black *et al.*[27] Only the carbon G band (1583 cm^{-1}) of HOPG is present in the Raman spectrum (Figure S11a). However in the FTIR a band for Na_2CO_3 at 1429 cm^{-1} (Figure S11b) is detected.

Observations from the AFM study are summarised within Schematic S1 where initially a thin film (2-3 nm) is formed on the surface with deposits of 5 nm nanoparticles. Platelets appear on the surface an order of magnitude (100 nm) bigger than the film. On the surface as you increase the over potential you see the agglomeration of cubic structures that grow into rectangular prisms of NaO_2 that consist of 8 discrete building blocks. The start of the oxidation process the edges of each crystal loses definition, leading to the presence of nano-agglomerates left at the interface. The resulting "ghost" shells of the crystal can be seen on the interface identified as Na_2CO_3.

Further AFM measurements (Figure S12) showed that NaO_2 crystallisation chemistry was found to be salt dependent and reduction of O_2 in 0.5M NaTFSI, DEGDME in the electrolyte resulted in the formation of a holed plate like deposit with larger dimensions of 16x16x0.5 μm. This identifies that further work need to be undertaken to fully understand the role of the anion, as well as ion coordination and solvent types in electrolytes on NaO_2 precipitation.[28]

The observation of imperfections on the NaO_2 rectangular prism including both holes and axial lines indicate the high mobility of NaO_2 particles at the interface to agglomerate and grow in discrete, potential dependent morphologies. This has implications for practical cells where controlling type of NaO_2 precipitate will be necessary for predictable cell behaviour. The high mobility of NaO_2 means that agglomerates will migrate along the surface until an energy favourable site, such as a defect, is available to deposit. At the initial stage of reduction the NaO_2 is dissolved into the electrolyte. Once the double layer is saturated with NaO_2, the deposition and formation of NaO_2 crystals can occur.

Evidence of coarsening or Ostwald ripening is exhibited in the initial film and final stages of the reduction of O_2 (Figure 1c) and oxidation of NaO_2 (Figure 1g). This is provided by the spherical nature of the particles mapped within the AFM images. These are thermodynamically more stable due to surface energy minimisation of the particles through particle dissolution and ion precipitation.[29] At this stage of formation the precipitation of primary nanoparticles is similar to classical nanoparticle growth. Therefore at these stages of the discharge, a high concentration of monomers i.e. O_2^- and Na^+ should prevent particle coarsening and changes in morphology.[30,31] These effects would be heightened at an electrode interface due to the formation of the double layer structure. The anion plays a considerable role in the structure of the double layer in each system, hence, the electrolyte anion affects these stages of NaO_2 growth, as demonstrated by the variation in deposit size between $NaClO_4$ (Figure 1) and NaTFSI (Figure S12). However, classical crystallisation does not characterise the complete mechanism here due to the observation of Rubik cube like structures.

Precursor layered plates and then Rubik cube like structures is unsurprising given observations of oxide formation in this solvent in the lithium analogue of this system.[20] From the evidence here the steps between spherical nanoparticles of NaO_2 and rectangular prismatic structures suggest a reoriented aggregation (RO) or mesocrystal mechanism is taking place. RO mechanisms simply encompass the aggregation of building block nanoparticles that then reorient to form single faced structures again minimising surface energy. It is observed within the film the initially formed NaO_2 nanoparticles (Figure 1c). These favourable aggregation sites will then form the precipitation sites at the interface. Here collisions of aligned nanocrystals in suspension or the rotation of collided misaligned nanoparticles form the basis of growth at the interface.[31,32] Once an agglomerate of a certain size is reached in some instances coarse ripening has been shown to smooth the edges of the final crystal structures. However, this model is not the best fit. Mesocrystal formation is a better model in this case because of the initial stages of growth proceeding into subsequent smoothing of the final precipitate. In mesocrystal formation the primary nanoparticles are iso-oriented into a crystal via oriented aggregation (OA).[33] Organic media has been shown to temporarily stabilise these particles and form a mesocrystal via mesoscale assembly.[33] Fusion can then occur to form an oriented crystal and then finally to a single crystal. These previous observations help to explain the observations of the Rubik cube like structures within this data series. Within this the final stage of fusion to form a single crystal is not observed (in contrast to many literature reports[33,34]), most likely due to the much shorter timescale of the voltammetry experiment and the high current rate generation of superoxide.

The process of meso-crystals fusion, which is thermodynamically favoured under the displacement of the solvent molecules can often include part of the organic molecule as a coating.[33] and this is proposed as a pathway for the formation of a Na_2CO_3 coating upon the crystals forming, and a crust of Na_2CO_3 remaining on the surface of the electrode after oxidation of NaO_2.[26]

The dissolution mechanism should firstly oxidise the surface layer in contact with the surface and the edges of the rectangular prism agglomerates. The stages characterised in this study would suggest that similar stages of dissolution are present upon dissolution as on formation of these mesocrystals.

The scan rate used (100 mVs^{-1}) resulted in a high rate of O_2 reduction leading to initial film formation from supersaturation of the double layer providing many smaller nucleation points.[35] In the medium ionic strength electrolyte ($NaClO_4$/DEGDME) the amount of time a particle of NaO_2 can reorient itself before being fixed, is lowered.[8] This observation is different to that reported by Ledrano *et al*[6] through *in situ* electrochemical quartz mass balance measurements upon Au electrodes. They concluded that there is only solution based NaO_2 in this instance and that no film is formed until the end of the discharge. Recently Lutz *et al*[36] have highlighted the different behaviour of this process due to substrate, especially the difference in observed morphology between carbon (cubic NaO_2) and Au (NaO_2 flakes) surfaces. Undoubtable the role of electrode surface, solvent, salt and H_2O level are play a major role on the growth and morphology of NaO_2 crystals and further investigations are required to understand these influences.

In conclusion*, ex situ* AFM images on HOPG demonstrate the rich and intricate dissolution and recrystallisation chemistry during O_2 reduction in an aprotic ether-based solvent in the presence of Na^+. An initial formation of a 5 nm NaO_2 film, followed by subsequent deposition of stacked NaO_2 platelets, is observed. These plates then grow into crystalline rectangular prisms (2x2x1 μm) consisting of 8 smaller sub-structures. These were found to preferentially agglomerate at the step edges of HOPG, but also upon the basal plane itself. The observation of building block rectangular prisms that have stacked on top of each other, with striations on the deposit resembling those found on the Rubik's Cube puzzle, was unexpected and this method of NaO_2 precipitation results in the observed 0.5 μm deep holes present in the central face of the NaO_2. Upon oxidation the dissolution of the rectangular prismatic structure, conserves an unevenly shaped collection of 8 sub-structures that degrades further to groups of 40 nm sized deposits. Rings of 200 nm diameter remain on the surface after oxidation, these rings are thought to be the un-oxidised side reaction product (Na_2CO_3) that forms upon the surface of NaO_2.

Support from the Engineering and Physical Sciences Research Council grant EP/J020265/1 and the Energy SuperStore, Early Career Researcher Award is acknowledged.

Notes and references

1 C. L. Bender, D. Schröder, R. Pinedo, P. Adelhelm and J. Janek, *Angew. Chem. Int. Ed.*, 2016, **55**, 4640–4649.

2 D. Schröder, C. L. Bender, M. Osenberg, A. Hilger, I. Manke and J. Janek, *Sci. Rep.*, 2016, **6**, 24288.

3 S. Y. Sayed, K. P. C. Yao, D. G. Kwabi, T. P. Batcho, C. V Amanchukwu, S. Feng, C. V Thompson and Y. Shao-Horn, *Chem. Comm.*, 2017, **53**, 460–460.

4 N. Ortiz-Vitoriano, T. P. Batcho, D. G. Kwabi, B. Han, N. Pour, K. P. C. Yao, C. V. Thompson and Y. Shao-Horn, *J. Phys. Chem. Lett.*, 2015, **6**, 2636–2643.

5 K. B. Knudsen, J. E. Nichols, T. Vegge, A. C. Luntz, B. D. McCloskey and J. Hjelm, *J. Phys. Chem. C*, 2016, **120**, 10799–10805.

6 I. Landa-Medrano, J. T. Frith, I. Ruiz de Larramendi, I. Lozano, N. Ortiz-Vitoriano, N. Garcia-Araez and T. Rojo, *J. Power Sources*, 2017, **345**, 237–246.

7 C. Xia, R. Black, R. Fernandes, B. Adams and L. F. Nazar, *Nat. Chem.*, 2015, **7**, 496–501.

8 J. E. Nichols and B. D. McCloskey, *J. Phys. Chem. C*, 2017, **121**, 85–96.

9 N. Zhao, C. Li and X. Guo, *Phys. Chem. Chem. Phys.*, 2014, **16**, 15646.

10 J. Kim, H. Park, B. Lee, W. M. Seong, H. D. Lim, Y. Bae, H. Kim, W. K. Kim, K. H. Ryu and K. Kang, *Nat. Commun.*, 2016, **7**, 10670–10679.

11 L. Lutz, W. Yin, A. Grimaud, D. Alves Dalla Corte, M. Tang, L. Johnson, E. Azaceta, V. Sarou-Kanian, A. J. Naylor, S. Hamad, J. A. Anta, E. Salager, R. Tena-Zaera, P. G. Bruce and J. M. Tarascon, *J. Phys. Chem. C*, 2016, **120**, 20068–20076.

12 I. M. Aldous and L. J. Hardwick, *Angew. Chemie - Int. Ed.*, 2016, **55**, 8254–8257.

13 B. Wang, N. Zhao, Y. Wang, W. Zhang, W. Lu, X. Guo and J. Liu, *Phys. Chem. Chem. Phys.*, 2017, **19**, 2940–2949.

14 J. Kim, H.-D. Lim, H. Gwon and K. Kang, *Phys. Chem. Chem. Phys.*, 2013, **15**, 3623.

15 I. I. Abate, L. E. Thompson, H. C. Kim and N. B. Aetukuri, *J. Phys. Chem. Lett.*, 2016, **7**, 2164–2169.

16 B. Wang, N. Zhao, Y. Wang, W. Zhang, W. Lu, X. Guo and J. Liu, *Phys. Chem. Chem. Phys.*, 2016, **19**, 2940–2949.

17 B. Sun, K. Kretschmer, X. Xie, P. Munroe, Z. Peng and G. Wang, *Adv. Mater.*, 2017, 1606816.

18 N. Zhao and X. Guo, *J. Phys. Chem. C*, 2015, **119**, 25319–25326.

19 X. Bi, R. Wang, L. Ma, D. Zhang, K. Amine and J. Lu, *Small Methods*, 2017, **1**, 1700102.

20 R. Wen, M. Hong and H. R. Byon, *J. Am. Chem. Soc.*, 2013, **135**, 10870–6.

21 C. Liu and S. Ye, *J. Phys. Chem. C*, 2016, **120**, 25246–25255.

22 L. Johnson, C. Li, Z. Liu, Y. Chen, S. A. Freunberger, P. C. Ashok, B. B. Praveen, K. Dholakia, J.-M. Tarascon and P. G. Bruce, *Nat. Chem.*, 2014, **6**, 1091–9.

23 S. E. Herrera, A. Y. Tesio, R. Clarenc and E. J. Calvo, *Phys. Chem. Chem. Phys.*, 2014, **16**, 9925–9929.

24 J. Kim, H.-D. Lim, H. Gwon and K. Kang, *Phys. Chem. Chem. Phys.*, 2013, **15**, 3623–9.

25 N. Ortiz-Vitoriano, T. P. Batcho, D. G. Kwabi, B. Han, N. Pour, K. P. C. Yao, C. V. Thompson and Y. Shao-Horn, *J. Phys. Chem. Lett.*, 2015, **6**, 2636–2643.

26 I. Landa-Medrano, A. Sorrentino, L. Stievano, I. Ruiz de Larramendi, E. Pereiro, L. Lezama, T. Rojo and D. Tonti, *Nano Energy*, 2017, **37**, 224–231.

27 R. Black, A. Shyamsunder, P. Adeli, D. Kundu, G. K. Murphy and L. F. Nazar, *ChemSusChem*, 2016, **9**, 1795–1803.

28 M. He, K. C. Lau, X. Ren, N. Xiao, W. D. McCulloch, L. A. Curtiss and Y. Wu, *Angew. Chem. Int. Ed.*, 2016, **55**, 15310–15314.

29 I. M. Lifshitz and V. V. Slyozov, *J. Phys. Chem. Solids*, 1961, **19**, 35–50.

30 X. Peng, L. Manna, W. Yang, J. Wickham, E. Scher, A. Kadavanich and A. P. Alivisatos, *Nature*, 2000, **404**, 59–61.

31 E. J. H. Lee, C. Ribeiro, E. Longo and E. R. Leite, *J. Phys. Chem. B*, 2005, **109**, 20842–20846.

32 C. Ribeiro, E. J. H. Lee, T. R. Giraldi, E. Longo, J. A. Varela and E. R. Leite, *J. Phys. Chem. B*, 2004, **108**, 15612–15617.

33 M. Niederberger and H. Cölfen, *Phys. Chem. Chem. Phys.*, 2006, **8**, 3271–3287.

34 J. Fang, B. Ding, X. Song and Y. Han, *Appl. Phys. Lett.*, 2008, **92**, 17120–17123.

35 L. C. Soare, P. Bowen, J. Lemaitre and H. Hofmann, *J. Phys. Chem. B*, 2006, **110**, 17763–17771.

36 L. Lutz, D. A. D. Corte, Y. Chen, D. Batuk, L. R. Johnson, A. Abakumov, L. Yate, E. Azaceta, P. G. Bruce, J.-M. Tarascon and A. Grimaud, *Adv. Energy Mater.*, 2017, 1701581.